


SCIENTIFIC REPORTS



OPEN

Polarization-entangled photon generation using partial spatially coherent pump beam

Yaseera Ismail¹, Stuti Joshi¹ & Francesco Petruccione^{1,2} 

The generation of two photon fields, to date, has been demonstrated utilizing a fully coherent pump beam. In this paper we demonstrate, the theoretical and experimental generation of polarization entangled single photon pairs by varying the spatial coherence of the pump beam. The effect of the pump beam spatial coherence on the visibility of a polarization-entangled single photon source is investigated. A comparison of the visibility measurements using a fully coherent and partially coherent pump beam is performed. It is shown that the partial coherence of the pump beam contributes to an increase in the visibility. The coherence properties of the beam are significant for free-space optical transmission in particular for long range free-space quantum communication.

The process of spontaneous parametric down-conversion (SPDC)¹ is the foremost popular method of producing entangled photons and has acquired immense attention of late due to its potential applications in quantum communication especially for long range free-space and satellite quantum key distribution²⁻⁴. Governed by the laws of conservation of energy and momentum, high frequency pump photons split into highly correlated low frequency photon pairs whereby the generated photon pairs form an entangled twin photon state^{4,5}. Photon pairs can be entangled in time and energy, phase and momentum and angular position and orbital angular momentum depending on the properties of the crystal and the pump beam. The aforementioned entanglement properties associated with the fourth-order correlation have been demonstrated in previous studies⁶⁻¹¹.

For many quantum applications, the two-photon interference effect corresponding to temporal^{12,8}, spatial^{13,14}, and angular interference^{15,16} has been demonstrated. Two-photon fields entangled in different degrees of freedom can provide additional resources to prepare the entangled quantum states for quantum communication.

The coherence properties of the entangled photon fields are affected by the pump properties and crystal parameters^{5,17-22}. In particular, the transfer of angular momentum of the pump beam²³ and the effect of the pump transverse width¹⁹ on the down-converted photons have been investigated both theoretically and experimentally. Thus far, entangled photons are experimentally generated by considering the pump beam to be fully spatially coherent (FSC). However, in many practical applications partially spatially coherent light demonstrated robustness over fully coherent light²⁴. Of late, there have been reports of theoretical studies focusing on integrating partial spatial coherence to an entangled photon field and studying the connection between the partial coherence and entanglement. For instance, the mathematical investigation of the duality between partial coherence and entanglement describes the propagation, diffraction and interference of bi-photon fields in optical linear systems²⁵. In particular, the beam properties such as spectral intensity and state of polarization are intrinsically connected to the spatial coherence of the pump beam²⁶.

The generation of the biphoton field is not limited to SPDC, it was recently shown that the process of four wave mixing within a hot Rubidium atomic vapor cell, resulted in the production of bright narrowband biphotons where a violation of the Cauchy-Schwartz inequality was demonstrated²⁷. It was also shown that within an atomic medium it is possible to study the effects of the temporal correlation by producing the narrowband biphoton field using frequency-bin entanglement²⁸.

In the present paper, applying the process of SPDC, we demonstrate a novel pump source for entangled photons by incorporating a scheme to produce partial spatial coherence of the pump beam. In doing so we achieve a varying partial spatial coherent pump photon source. We show for the first time the partially spatially coherent source for a quantum system. An experimental study is performed to investigate the effects of the pump spatial coherence, on the properties of the polarization-entangled photon field. We observe the non-classical behaviour

¹University of KwaZulu-Natal, School of Chemistry and Physics, Quantum Research Group, Durban, 4000, South Africa. ²National Institute for Theoretical Physics (NITheP), KwaZulu-Natal, South Africa. Correspondence and requests for materials should be addressed to Y.I. (email: Ismaily@ukzn.ac.za)

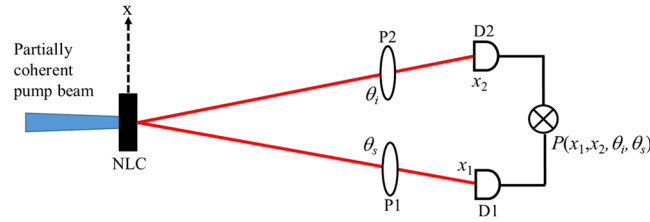


Figure 1. Schematic setup used to study the influence of the pump spatial coherence on the polarization entangled photons.

of the two-photon field for different values of the pump spatial coherence lengths by testing the visibility and the Clauser, Horne, Shimony and Holt (CHSH) inequality²⁹. Furthermore, the associated measurements were performed on the conventional coherent pump source (FSC) and compared with the partially spatially coherent pump beam. Since the state of polarization and coherence are intimately connected³⁰, it can be expected that the polarization properties are influenced by the coherence. The present study is significant for potential applications in quantum information processing for free-space quantum communication.

Theoretical Background

Throughout the paper, subscripts p , s , and i stand for pump, signal, and idler respectively. The two-photon state $|\Psi\rangle$ generated by a partial spatial coherent pump source, as shown in Fig. 1, is expressed as²⁶,

$$|\Psi\rangle = A \exp(i\Delta k L/2) \iint dq_s dq_i V_p(q_p) \exp(i\Delta q L/2) \text{sinc}(\Delta q L/2) \hat{b}_s^\dagger(q_s) \hat{b}_i^\dagger(q_i) |0, 0\rangle, \quad (1)$$

where $|0, 0\rangle$ is the vacuum state, L is the length of the nonlinear crystal and $V_p(q_p)$ is the strength of the pump field with $q_p = q_s + q_i$ is the transverse coordinate of the wave-vector \mathbf{k}_p of the pump beam. For the paraxial approximation Δk and Δq are given by,

$$\Delta k = k_p - k_s - k_i, \quad (2a)$$

$$\Delta q = \frac{q_p^2}{2k_p} - \frac{q_s^2}{2k_s} - \frac{q_i^2}{2k_i}, \quad (2b)$$

where k_p , k_s and k_i are the wavenumber of the pump, the signal and the idler respectively. For $\Delta q < 0$, $\text{sinc}(\Delta q L/2) = \exp(-\gamma \sqrt{|\Delta q|^2} L/2)$ and $\gamma = 0.455$ ³¹.

For the theoretical calculation we considered partially coherent pump beam of Gaussian Schell-Model type. The correlation function for the Gaussian Schell-Model pump beam field is given by³²,

$$\langle V(\rho_1) V^*(\rho_2) \rangle = A_p^2 \exp\left\{ -\frac{\rho_1^2 + \rho_2^2}{2\sigma^2} - \frac{(\rho_2 - \rho_1)^2}{4\delta^2} \right\}, \quad (3)$$

where ρ_1 and ρ_2 are two transverse points in the source plane.

The probability of coincidence of the signal at x_1 and the idler at x_2 is given by²⁵,

$$P(x_1, x_2, \theta_s, \theta_i) = |\Psi\rangle E_s^-(x_1, \theta_s) E_i^-(x_2, \theta_i) E_i^+(x_2, \theta_i) E_s^+(x_1, \theta_s) |\Psi\rangle, \quad (4)$$

where $E_s^+(x, \theta_s)$ and $E_i^+(x, \theta_i)$ denote the positive frequency parts of the electric fields of the signal and the idler arriving at detectors D1 and D2 respectively. Similarly, $E_s^-(x, \theta_s)$ and $E_i^-(x, \theta_i)$ represent the negative frequency parts, θ_s and θ_i are the polarization angles of polarizers P1 and P2 inserted in the path of the signal and the idler field respectively. The positive and negative frequency parts of the signal and the idler at the detection plane can be expressed as²⁵,

$$E_j^+(x, \theta_j) = \cos(\theta_j) \int dq_j H_j(x, q_j) \hat{b}_j(q_j), \quad (5a)$$

$$E_j^-(x, \theta_j) = \cos(\theta_j) \int dq_j H_j^*(x, q_j) \hat{b}_j^\dagger(q_j), \quad (5b)$$

where $\hat{b}_j(q_j)$ and $\hat{b}_j^\dagger(q_j)$ are the annihilation and creation operator respectively and $j = s, i$. Here, $H_j(x, q_j)$ is the response of the signal (idler) system in free-space.

Substituting Equations (1), (2) and (5) into Equation (4) we obtained an expression for probability of coincidence detection of signal and idler in terms of pump cross-spectral density function as given by,

$$P(x_1, x_2, \theta_s, \theta_i) = |A|^2 \cos^2(\theta_s) \cos^2(\theta_i) \int \int \int \int d\rho_s d\rho'_s d\rho_p d\rho'_p W(\rho_s, \rho'_s, \rho_p, \rho'_p) \times \langle h_s(x_1, \rho_s) h_s^*(x_1, \rho'_s) h_i(x_2, \rho_p) h_i^*(x_2, \rho'_p) \rangle, \tag{6}$$

where, $\langle \dots \rangle$ is the ensemble average over all the realizations of the transverse coordinates, $h_j(x, \rho_j)$ is the Fourier transform of $H_j(x, q_j)$ with respect to ρ_j , and $W(\rho_s, \rho'_s, \rho_p, \rho'_p)$ is the cross-spectral density function of the partially coherent pump field which is the function of the ensemble average of the pump field over different realizations. The Fourier transform function $h_j(x, \rho_j)$ of $H_j(x, q_j)$ is given by,

$$h_j(x, \rho_j) = \sqrt{-\frac{ik_j}{2\pi z}} \exp\left(\frac{ik_j}{2z}(x - \rho_j)^2\right). \tag{7}$$

The cross-spectral density function $W(\rho_s, \rho'_s, \rho_p, \rho'_p)$ is given by,

$$W(\rho_s, \rho'_s, \rho_p, \rho'_p) = \frac{4\pi k_p}{L\sqrt{\gamma^2 + 1}} \left\langle V_p\left(-\frac{\rho_s + \rho_i}{2}\right) V_p^*\left(-\frac{\rho'_s + \rho'_i}{2}\right) \right\rangle \times \exp(-b(\rho'_s - \rho_i)^2 - c(\rho_s - \rho_i^2)), \tag{8}$$

where,

$$b = \frac{k_p}{4L(-i + \gamma)}, \tag{9a}$$

and

$$c = \frac{k_p}{4L(i + \gamma)}. \tag{9b}$$

Here $\left\langle V_p\left(-\frac{\rho_s + \rho_i}{2}\right) V_p^*\left(-\frac{\rho'_s + \rho'_i}{2}\right) \right\rangle$ represents the correlation function of the partially coherent pump beam and can be calculated using Equation (3) as,

$$\left\langle V_p\left(-\frac{\rho_s + \rho_i}{2}\right) V_p^*\left(-\frac{\rho'_s + \rho'_i}{2}\right) \right\rangle = A_p^2 \exp(-\eta(\rho_s + \rho_i)^2 - \eta(\rho'_s + \rho'_i)^2 + \eta'(\rho_s + \rho_i)(\rho'_s + \rho'_i)), \tag{10}$$

where,

$$\eta = \frac{1}{16\delta^2} + \frac{1}{8\sigma^2}, \tag{11a}$$

$$\eta' = \frac{1}{8\delta^2}, \tag{11b}$$

A_p^2 is a constant, σ and δ represents the beam waist and the pump coherence length respectively. Substituting Equations (7), (8) and (10) into Equation (6) and after some calculation the probability of coincidence detection can be expressed as,

$$P(x_1, x_2, \theta_s, \theta_i) = \frac{C \cos^2(\theta_s) \cos^2(\theta_i)}{\sqrt{(2A_1(-a + c + \eta)^2(a - 2c)^2(a - 2\eta)(A_2 + A_3 - 2a^2x_2))}} \times \exp\left(\frac{a^2x_1^2}{-a + c + \eta}\right) \exp\left(\frac{a^2(x_1(2a - 4\eta + \eta') + x_2\eta')^2}{2A_1(a - 2\eta)}\right) \times \exp\left(\frac{4a^2(-ax_2 + c(x_1 + x_2) + (x_2 - x_1)\eta)^2}{4A_1(a - 2c)(A_3 - 2a^2x_2 + A_2)}\right) \times \exp\left(\frac{(a\eta'A_1(x_1 - x_2) - 2a(b - \eta)(a - 2c)(x_1(2a - 4\eta + \eta') + x_2\eta'))^2}{4A_1(a - 2c)(A_3 - 2a^2x_2 + A_2)}\right), \tag{12}$$

where $a = ik_p/4z$ and A_1, A_2, A_3 can be expressed in terms of a, b, c, η, η' .

$$A_1 = 2a^2 + 2a(b - \eta) - 4b\eta - 4\eta^2 + \eta'^2, \tag{13a}$$

$$A_2 = \frac{2a^2 + 2ab - 4ac - 4bc + 2a\eta - 4c\eta + \eta'^2}{2(a - 2c)}, \tag{13b}$$

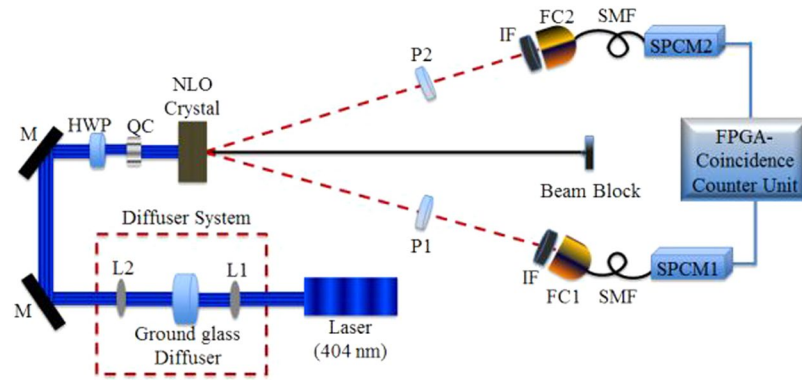


Figure 2. Schematic of an entangled photon source comprising of a pump laser lasing as 405 nm, diffuser system containing a ground glass diffuser and lens system, mirrors (M), a Half Wave Plate (HWP), a Quartz Crystal (QC), BBO crystal, a polarizer in each arm followed by infra-red filters (IF) and a fiber coupler connected to single photon detectors (SPCM1 and SPCM2) via polarization maintaining fibers to the in-house coincidence counting unit (CCU) comprising of a Field Programmable Gated Array (FPGA).

$$A_3 = -\frac{2(a - 2\eta)(b - \eta)^2}{A_1}. \quad (13c)$$

Equation (12) shows the probability of coincidence detection for polarization entangled photons as a function of different parameters. The parameter C is a function of k , z and γ , which were kept constant during the experiment. The wavelength of the pump beam $\lambda = 405$ nm, length of the nonlinear crystal $L = 7$ mm and the distance between nonlinear crystal and detectors $z = 500$ mm. The visibilities of the polarization entangled photons for different values of the pump coherence lengths were calculated by fixing the aforementioned parameters using Equation (12). The coincidence counts were determined under the condition that both the detectors (D1 and D2) are fixed at $x_1 = x_2 = 0$. For the visibility measurements, polarizer, P1, is at $\theta_1 = 0^\circ$ and 45° (rectilinear and diagonal basis respectively) while the polarizer, P2, is rotated from $\theta_2 = 0$ to 2π .

Experimental Setup

To reproduce the entanglement scheme incorporating the novelty of the partial spatial coherent pump, we implement the process of SPDC utilizing a nonlinear crystal in a type-I concatenated configuration as presented in Fig. 2. The partial spatial coherence applied to the quantum system was investigated by means of performing measurements in the polarization degree of freedom.

The partially spatially coherent (PSC) pump beam was implemented by propagating the initial pump beam (405 nm) through a rotating ground glass diffuser (Fig. 2). A collection lens ($L_2 = 50$ mm) was used to collimate the pump beam coming out of the diffuser. The spatial coherence length was varied by varying the size of the beam incident on the diffuser whereby the coherence length was calculated by, $\delta = \frac{3.832\lambda}{2\pi d}$ ³³, where λ is the wavelength of the pump beam, f is the focal length of lens L_2 and d is the diameter of the beam imposed onto the ground glass diffuser. Non-collinear photon pairs at a down-converted wavelength of 810 nm were produced by two type-I Beta Barium Borate (BBO) crystals ($7 \times 7 \times 0.7$ mm) concatenated using a partially coherent pump beam laser lasing at 405 nm. A quartz crystal (QC) was used to remove unwanted phase shifts. The polarization of the pump beam was controlled using a half wave plate (HWP) which was set to diagonally polarized light relative to the BBO axes allowing for an equal probability of horizontal and vertical polarized photons being generated (signal and idler) in accordance to the state

$$|\Psi\rangle = \frac{1}{\sqrt{2}}[|V_s\rangle|V_i\rangle + \exp(-i\phi)|H_s\rangle|H_i\rangle], \quad (14)$$

where, $|V\rangle$ and $|H\rangle$ are the vertical and horizontal states respectively and ϕ is the phase difference. Since the source was built to perform measurements in the polarization degree of freedom, a linear polarizer was placed in each of the free arms (signal and idler) for measurement purposes. The single photons were collected using free-space to fiber couplers containing a collecting lens with a focal length of 11 mm. Single mode fibers (SMF) were used to couple from the fiber couplers to the single photon avalanche detectors/modules (SPCM) with efficiencies of 65% and dark count rates of the order 100/sec. Coincidence detection was acquired using a multi-channel Coincidence-Counting Unit (CCU) comprising of integrated circuit components. The signals from the SPCM registered as inputs in the CCU, which were a combination of random 2-fold coincidences. The pulses registered as two outputs into a field programmable gate array (FPGA). Coincidence counts were obtained for integration time intervals ranging from 1 s to 5 s for better accuracy within a time window of 7 ns

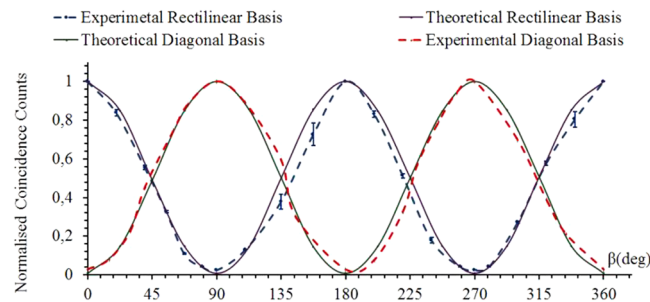


Figure 3. Correlation fringes for the rectilinear ($\alpha = 0^\circ$) and diagonal basis ($\alpha = 45^\circ$) while varying the orientation of the second polarizer ($\beta: 0^\circ$ to 360°) for the pump beam coherence length of $112 \mu\text{m}$.

Pump Beam Size	Pump Beam Coherent Length	Rectilinear Basis	Diagonal Basis	Theoretical Visibility
—	FSC	$90.1 \pm 1.3 \%$	$90.6 \pm 1.3 \%$	97%
$110 \mu\text{m}$	$112 \mu\text{m}$	$95.1 \pm 3.4 \%$	$94.7 \pm 3.9 \%$	98.5%
$350.5 \mu\text{m}$	$35 \mu\text{m}$	$95.8 \pm 2.9 \%$	$95.6 \pm 3.1 \%$	98.7%
$456.8 \mu\text{m}$	$27 \mu\text{m}$	$96.9 \pm 3.1 \%$	$97.1 \pm 2.8 \%$	98.9%

Table 1. Visibility obtained from the correlation fringes for the rectilinear ($\alpha = 0^\circ$) and diagonal basis ($\alpha = 45^\circ$) for a FSC beam and varying coherence length of the PSC beam.

Results and Discussion

The coherence length was varied for different magnitudes of partial spatial coherence and determined by measuring the beam diameter at the plane of the ground glass diffuser. Coherence lengths ranging from $27 \mu\text{m}$ to $112 \mu\text{m}$ were achieved.

To verify that our partially spatially coherent source was producing entangled photons, we first and foremost analyzed the correlation fringes for the rectilinear and diagonal basis by setting the linear polarizer P1, α to 0° and 45° respectively while varying the orientation of the second polarizer P2, $\beta: 0^\circ$ to 360° .

The normalized coincidence counts obtained from the experimental data is plotted in Fig. 3 for the pump coherence length of $112 \mu\text{m}$. As expected the coincidence counts showed a sinusoidal behavior. A high fringe visibility of $95.1 \pm 3.4\%$ and $94.7 \pm 3.9\%$ was obtained for the rectilinear (dashed blue curve) and diagonal basis (dashed red curve) respectively. The corresponding theoretical visibility fringes for the rectilinear and the diagonal basis using Equation (12) are plotted by the purple and green solid curves respectively. The experimental visibility curves follow the same trends as the theoretical curves (as per Equation (12)). However, there is a slight shift in the position of maximum and minimum coincidence counts which is due to slight misalignment in the experimental setup. To characterize the source robustness, the visibility of the polarization photons were measured for different values of the pump beam coherence lengths. The results of the experimental visibilities for the FSC and varying coherence lengths of PSC are presented in Table 1, including the corresponding theoretically calculated visibility attained from Equation (12). From these results, it was observed that the visibility of the coincidence fringes increases as the spatial coherence length of the pump beam decreases. The coherence lengths were varied by varying the pump beam size at the plane of the ground glass diffuser. As the beam size decreases the wave-function becomes more separable resulting in an increase of the field coherence length²⁵. Due to this the field becomes less entangled and therefore the visibility is lower as proposed theoretically by Saleh *et al.*²⁵. The decrease in the visibility of the biphoton field with respect to varying pump coherence length is shown in Table 1. Our results agree with the theoretical studies based on the aforementioned paper²⁵ and relate the fringe visibility of the entangled photons to the spatial coherence of the pump beam. For the coherence length of $112 \mu\text{m}$ (higher coherence, smaller beam size) the visibility obtained is less than that obtained for $27 \mu\text{m}$ (less coherence, larger beam size). The theoretical model predicts a small change in the visibility with the variation of pump spatial coherence length. The visibility measurements obtained are also influenced by the pump beam waist and the pump coherence length.

The aforementioned parameters were determined experimentally and adopted into the theoretical model for both cases, PSC and FSC.

The verification of entanglement lies in the violation of the CHSH inequality performed by determining the expected correlation of entanglement. Therefore a measurement of CHSH was performed for different values of the pump coherence lengths. The coincidence counts were recorded for 5 s. The following set of optimum polarization orientations were chosen for the linear polarizer $\alpha = 0^\circ$, $\alpha' = 45^\circ$, $\beta = 22.5^\circ$ and $\beta' = 67.5^\circ$. Four sets of

Pump Beam Coherent Length	CHSH Inequality	Percentage(%)
FSC	2.70	2.0
112 μm	2.76	0.2
35 μm	2.77	0.2
27 μm	2.78	0.2

Table 2. Measured violation of the CHSH inequality for the fully (FSC) and varying values of coherence length of the partially spatially coherent (PSC) pump beam.

experimental runs were conducted corresponding to the four sets of expectation values in the definition of the CHSH inequality²⁹ and the overall results are presented in Table 2 for the fully and partially spatially coherent pump beam.

These results show that for the coherence length of 112 μm , the CHSH inequality parameter obtained was $S = 2.76$ with a percentage error of 0.2 which according to the local realism theory is $|S| < 2$ and $2 < |S| \leq 2\sqrt{2}$ according to theoretical limit of quantum mechanics. As performed previously, the robustness of the system was determined in terms of the CHSH inequality for various values of the pump beam coherence lengths. The results obtained in Table 2 show that the degree of entanglement increases with the decrease of the pump spatial coherence. Compared to alternative methods of producing the biphoton field such as frequency-bin entanglement within an atomic medium²⁸, the SPDC source presented here, has a stronger violation of the CHSH Inequality. It is worth noting however that within the atomic medium it is possible to produce triplet fields by the process of parametric amplification six-wave mixing. Although these fields are weaker than the biphoton field, it provides opportunities to engineer three-channel entangled imaging on a chip³⁴.

Conclusion

The effects of spatial coherence of the pump beam on an entangled single photon source was studied. The PSC pump beam measured a higher visibility and CHSH inequality in comparison to the FSC pump beam. The experimental results showed that it is possible to obtain a tunable polarization entangled photon source by tailoring the pump beam coherence length. Of late, it has been shown theoretically that the detection probability of the two-photon field generated by the partially spatially coherent pump beam is higher and less susceptible to atmospheric turbulence than the two-photon field produced by the fully spatially coherent pump beam³⁵. We have recently demonstrated the effects that the fully spatially coherent pump beam undergoes when passed through various strengths of atmospheric turbulence³⁶. In this study we showed that the detection scheme of the single photon source is influenced by the changes in the atmospheric turbulence due to the breakdown of the spatial modes. Here, we showed for the first time the partially spatially coherent source for a quantum system. The present study might be useful for the preparation of two-qubit states by considering the partial spatial coherence of the pump beam for the application of free-space quantum communication. The coherence properties of the pump beam can be engineered to produce maximally entangled states³⁷. This infers that a PSC pump beam within an entangled single photon source is a promising pump source in the application of free-space quantum communication.

References

- Burnham, D. C. & Weinberg, D. L. Observation of simultaneity in parametric production of optical photon pairs. *Physical Review Letters* **25**, 84 (1970).
- Ursin, R. *et al.* Entanglement-based quantum communication over 144 km. *Nature physics* **3**, 481–486 (2007).
- Wang, J.-Y. *et al.* Direct and full-scale experimental verifications towards ground-satellite quantum key distribution. *Nature Photonics* **7**, 387–393 (2013).
- Yin, J. *et al.* Quantum teleportation and entanglement distribution over 100-kilometre free-space channels. *Nature* **488**, 185–188 (2012).
- Hong, C. & Mandel, L. Theory of parametric frequency down conversion of light. *Physical Review A* **31**, 2409 (1985).
- Klyshko, D. N. *Photons Nonlinear Optics* (CRC Press, 1988).
- Franson, J. D. Bell inequality for position and time. *Physical Review Letters* **62**, 2205 (1989).
- Kwiat, P. G., Steinberg, A. M. & Chiao, R. Y. High-visibility interference in a bell-inequality experiment for energy and time. *Physical Review A* **47**, R2472 (1993).
- Brendel, J., Gisin, N., Tittel, W. & Zbinden, H. Pulsed energy-time entangled twin-photon source for quantum communication. *Physical Review Letters* **82**, 2594 (1999).
- Rarity, J. & Tapster, P. Experimental violation of bell's inequality based on phase and momentum. *Physical Review Letters* **64**, 2495 (1990).
- Walborn, S., De Oliveira, A., Thebaldi, R. & Monken, C. Entanglement and conservation of orbital angular momentum in spontaneous parametric down-conversion. *Physical Review A* **69**, 023811 (2004).
- Brendel, J., Mohler, E. & Martienssen, W. Time-resolved dual-beam two-photon interferences with high visibility. *Physical review letters* **66**, 1142 (1991).
- Ghosh, R. & Mandel, L. Observation of nonclassical effects in the interference of two photons. *Physical Review Letters* **59**, 1903 (1987).
- Fonseca, E., da Silva, J. M., Monken, C. & Pádua, S. Controlling two-particle conditional interference. *Physical Review A* **61**, 023801 (2000).
- Mair, A., Vaziri, A., Weihs, G. & Zeilinger, A. Entanglement of the orbital angular momentum states of photons. *Nature* **412**, 313–316 (2001).
- Oemrawsingh, S. *et al.* Experimental demonstration of fractional orbital angular momentum entanglement of two photons. *Physical review letters* **95**, 240501 (2005).
- Rubin, M. H. Transverse correlation in optical spontaneous parametric down-conversion. *Physical Review A* **54**, 5349 (1996).

18. Monken, C. H., Ribeiro, P. S. & Pádua, S. Transfer of angular spectrum and image formation in spontaneous parametric down-conversion. *Physical Review A* **57**, 3123 (1998).
19. Joobeur, A., Saleh, B. E., Larchuk, T. S. & Teich, M. C. Coherence properties of entangled light beams generated by parametric down-conversion: Theory and experiment. *Physical Review A* **53**, 4360 (1996).
20. Ribeiro, P. S. Partial coherence with twin photons. *Physical Review A* **56**, 4111 (1997).
21. Fonseca, E., Monken, C., Pádua, S. & Barbosa, G. Transverse coherence length of down-converted light in the two-photon state. *Physical Review A* **59**, 1608 (1999).
22. Saleh, B. E., Teich, M. C. & Sergienko, A. V. Wolf equations for two-photon light. *Physical review letters* **94**, 223601 (2005).
23. Jha, A. K. *et al.* Angular two-photon interference and angular two-qubit states. *Physical review letters* **104**, 010501 (2010).
24. Gbur, G. & Wolf, E. Spreading of partially coherent beams in random media. *JOSA A* **19**, 1592–1598 (2002).
25. Saleh, B. E., Abouraddy, A. F., Sergienko, A. V. & Teich, M. C. Duality between partial coherence and partial entanglement. *Physical Review A* **62**, 043816 (2000).
26. Jha, A. K. & Boyd, R. W. Spatial two-photon coherence of the entangled field produced by down-conversion using a partially spatially coherent pump beam. *Physical Review A* **81**, 013828 (2010).
27. Zhu, L., Guo, X., Shu, C., Jeong, H. & Du, S. Bright narrowband biphoton generation from a hot rubidium atomic vapor cell. *Applied Physics Letters* **110**, 1–4 (2017).
28. Guo, X., Mei, Y. & Du, S. Testing the bell inequality on frequency-bin entangled photons using time-resolved detection. *Optica* **4**, 388–392 (2017).
29. Clauser, J. F., Horne, M. A., Shimony, A. & Holt, R. A. Proposed experiment to test local hidden-variable theories. *Physical review letters* **23**, 880 (1969).
30. Wolf, E. Unified theory of coherence and polarization of random electromagnetic beams. *Physics Letters A* **312**, 263–267 (2003).
31. Chan, K., Torres, J. & Eberly, J. Transverse entanglement migration in hilbert space. *Physical Review A* **75**, 050101 (2007).
32. Mandel, L. & Wolf, E. *Optical coherence and quantum optics* (Cambridge university press, 1995).
33. Foley, J. T. Effect of an aperture on the spectrum of partially coherent light. *JOSA A* **8**, 1099–1105 (1991).
34. Li, C. *et al.* Controlled correlation and squeezing in prysio to yield correlated light beams. *Physical Review Applied* **7**, 1–9 (2017).
35. Qiu, Y. & She, W. The influence of atmospheric turbulence on partially coherent two-photon entangled field. *Applied Physics B* **108**, 683–687 (2012).
36. Ismail, Y., Joshi, S., Forbes, A. & Petruccione, F. Instrumentation limitation of an polarization-based entangled photon source. *Journal of Optical Sociey of America B* **34**, 1084–1089 (2017).
37. Olvera, M. A. & Franke-Arnold, S. Two photon amplitude of partially coherent partially entangled electromagnetic fields. *arXiv preprint arXiv:1507.08623* (2015).

Acknowledgements

This work is based on research supported by the South African Research Chair Initiative of the Department of Science and Technology and National Research Foundation.

Author Contributions

The manuscript contribution is as follows, Y.I. conceived the experiment. Y.I. and S.J. conducted the experiments, theory and analysed the results. All authors reviewed the manuscript.

Additional Information

Competing Interests: The authors declare that they have no competing interests.

Publisher's note: Springer Nature remains neutral with regard to jurisdictional claims in published maps and institutional affiliations.



Open Access This article is licensed under a Creative Commons Attribution 4.0 International License, which permits use, sharing, adaptation, distribution and reproduction in any medium or format, as long as you give appropriate credit to the original author(s) and the source, provide a link to the Creative Commons license, and indicate if changes were made. The images or other third party material in this article are included in the article's Creative Commons license, unless indicated otherwise in a credit line to the material. If material is not included in the article's Creative Commons license and your intended use is not permitted by statutory regulation or exceeds the permitted use, you will need to obtain permission directly from the copyright holder. To view a copy of this license, visit <http://creativecommons.org/licenses/by/4.0/>.

© The Author(s) 2017